Wave trapping by acoustic black hole: Simultaneous reduction of sound reflection and transmission

Yongzhen Mi, Wei Zhai, Li Cheng, Chenyang Xi, and Xiang Yu

View Online   Export Citation   CrossMark

Wave trapping by acoustic black hole: Simultaneous reduction of sound reflection and transmission

Yongzhen Mi,[1] (iD) Wei Zhai,[2] (iD) Li Cheng,[3] (iD) Chenyang Xi,[4] and Xiang Yu[1,a)] (iD)

AFFILIATIONS

[1]Institute of High Performance Computing, A*STAR, 138632 Singapore
[2]Department of Mechanical Engineering, National University of Singapore, 117411 Singapore
[3]Department of Mechanical Engineering, The Hong Kong Polytechnic University, 999077 Hong Kong
[4]State Key Laboratory of Mechanical System and Vibration, Institute of Vibration, Shock and Noise, Shanghai Jiao Tong University, 200240 Shanghai, China

Note: This Paper is part of the APL Special Collection on Metastructures: From Physics to Applications.
[a)]Author to whom correspondence should be addressed: yuxiang@ihpc.a-star.edu.sg

ABSTRACT

Reduction of vibration and sound energy in the form of traveling waves is of vital importance in many applications. Recent development of acoustic metamaterials opens up unusual ways for sound wave manipulation and control. Among acoustic metamaterials, a much newer concept, Acoustic Black Hole (ABH), has been drawing growing attention in recent years, which shows great potential for acoustic energy trapping and dissipation. In a duct ABH with a properly tailored continuous cross-sectional reduction and impedance variation, it is shown that the sound speed can be progressively reduced, which means that sound waves are eventually trapped in the structure. In this paper, such a wave trapping mechanism is further explored in the context of sound transmission problems, in which an exceptional phenomenon—simultaneous reduction of sound reflection and transmission—is realized. The archived trapping mechanism also ensures that little sound waves will be bounced back to the source to jeopardize the overall performance. Transfer matrix method simulations and impedance tube experiments are performed to characterize the behavior of such a structure and to validate the theory. The promising ABH-specific features arising from the proposed design could overcome many existing limitations of traditional noise control devices.

An Acoustic Black Hole (ABH) has recently emerged as a fascinating concept to passively control acoustic wave propagation in structures or fluids.[1] The idea was first proposed in the study of a retarding beam structure,[2] whose termination is tapered following a power-law thickness profile. A nonreflecting edge condition can be realized as the incoming wave velocity is progressively reduced to zero. As a result, waves can never reach the end to be reflected back.[3] The idealized scenario describes that a wedge with its thickness perfectly reduced to zero at the end of the taper becomes a singularity for incoming waves, giving rise to the term "acoustic black hole." As energy is conservative, the wave energy trapped in the structure will unboundedly increase the vibration amplitude if no damping exists, especially in the structural tip region. However, previous studies have shown that even a small truncation at the tip could greatly compromise the ideal ABH effect.[4] This can, however, be alleviated by applying additional damping treatment. With the deployment of a small amount of damping material such as viscoelastic coating over the tip area, the ABH-induced high energy concentration would enable effective dissipation of the wave energy.[5] Characteristics of wave propagation,[6,7] effects of structural parameters on the ABH effect,[8] and sound transmission through plates with embedded ABH indentations[9] have been extensively discussed. Recent studies also extended the classical ABH design by curling the tip to a spiral shape,[10] and replaced the free damping layer by a constrained one.[11]

Most existing studies have been focusing on flexural waves in structures, such as beams and plates. Our motivation is to utilize the slow-sound effect of the ABH to control sound waves in fluids. The promising features of sound trapping could overcome many limitations of traditional duct absorbers such as Helmholtz resonators[12,13] or MPP absorbers.[14,15] Pioneering work by Mironov[16] analyzed a

one-dimensional duct ABH, inside which annular rings are placed to gradually reduce the sound speed along the waveguide. The Transfer Matrix Method (TMM)[17,18] was later employed to study linear and quadratic profiles of rings, where the parametric effects such as the ABH length, discretization of the rings, and damping loss factors have been discussed. These pioneering works theoretically proved the existence of the slow-sound effect, which is similar to rainbow trapping metamaterials.[19–21] Preliminary experimental investigations were also conducted to verify the ability of the ABH to minimize reflections in an acoustic duct.[22] Despite this effort, it is recognized that the sonic ABH is much less understood compared to its vibrational counterpart. Different characteristics of structural waves in solid and acoustic waves in fluid medium also demand more in-depth investigations. In addition, whether simultaneous realization of reduced energy transmission in a duct can be achieved through proper sonic ABH design and its interplay with the specific wave trapping remains an important question to be answered.

This study investigates the sound transmission characteristics through an open-end ABH in a circular duct, whose inner radius undergoes a continuous quadratic variation. The general concept is schematically illustrated in Fig. 1. As sound waves impinge from different directions, the sound speed will progressively be slowed down through their interactions with the ABH structure. This process would entail a significant reduction in the acoustic energy escaping from the ABH. Different from the dead-end configuration, which aims at realizing perfect absorption, the configuration under investigation in this work has an open end, whose acoustic admittance is not zero, which allows sound to transmit through the ABH. We anticipate that if an open-end ABH preserves the physical behavior of a conventional ABH, it can simultaneously enable a low sound reflection and transmission, which is the most desirable feature in sound control.

In what follows, we first derive analytical expressions governing the wavenumber and sound speed of propagating waves inside the proposed structure. The derivations take into account the open-end section whose radius is not completely decayed to zero. We show that if the ratio between the inlet and outlet radii is large enough, the shrinking duct still preserves the slow-sound effect. Then, the actual reflection and transmission characteristics of the duct ABH are
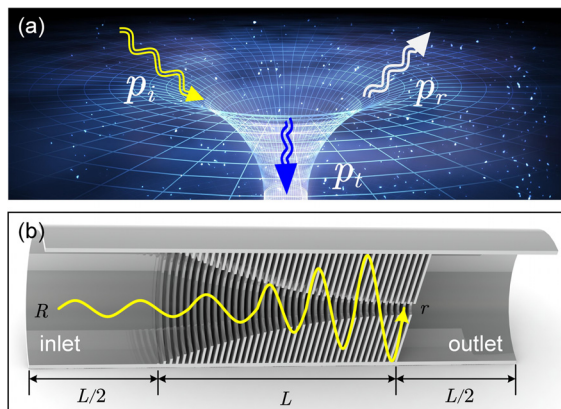
determined using TMM calculations. It is shown that the sound reflection coefficient rapidly decreases as the sound energy is trapped inside the structure. Both reflection and transmission coefficients can be simultaneously reduced, leading to an open-end device with nearly no reflection and transmission.

Consider the sound propagation inside an ABH structure as depicted in Fig. 2, in which the inner rings follow a decreasing power-law trend. It is connected to a circular duct of radius R, ended by an aperture of radius r. The generalized Webster equation governing the sound propagation in the ABH structure is written as:[16–18]

$$\frac{\partial^2 p}{\partial x^2} + \frac{\partial p}{\partial x}\frac{\partial(\ln S(x))}{\partial x} + p\left(k_0^2 + j\rho_0\omega\frac{2Y(x)}{h(x)}\right) = 0, \quad (1)$$

where p is the acoustic pressure, ω is the angular frequency, $k_0 = \omega/c_0$ is the wavenumber, and ρ_0 and c_0 are the density and sound speed of air, respectively. $h(x)$ and $S(x)$ are the radius and the cross-sectional area of the circular duct at position x, $S(x) = \pi h^2(x)$. $Y(x)$ is the wall admittance, which is given by

$$Y(x) = -\frac{j\omega}{\rho_0 c_0^2}\frac{R^2 - h^2(x)}{2h(x)}. \quad (2)$$

The radius of the inner rings is assumed to follow a quadratic decay function as

$$h(x) = \frac{R-r}{L^2}x^2 + r, \quad (3)$$

where R is the initial duct radius at the entrance, $x=-L$; r is the residual radius of the open aperture at duct termination, $x=0$.

Substituting the wall admittance Eq. (2) and ring radius function Eq. (3) into Eq. (1) transforms the governing equation to

$$\frac{\partial^2 p}{\partial x^2} + \frac{\partial p}{\partial x}\left[\frac{4(R-r)x}{(R-r)x^2 + rL^2}\right] + k_0^2 p\left[\frac{RL^2}{(R-r)x^2 + rL^2}\right]^2 = 0. \quad (4)$$

Assuming that the sound pressure takes a general expression of $p(x) \sim e^{jkx}$, the local wavenumber can be derived as

$$k(x) = \frac{\sqrt{k_0^2 R^2 L^4 - 4(R-r)^2 x^2}}{(R-r)x^2 + rL^2}. \quad (5)$$

FIG. 1. (a) Physical behavior of the ABH subjected to sound wave incidences. (b) Conceptual design of an open-end ABH in a one-dimensional duct to minimize sound transmission and reflection.
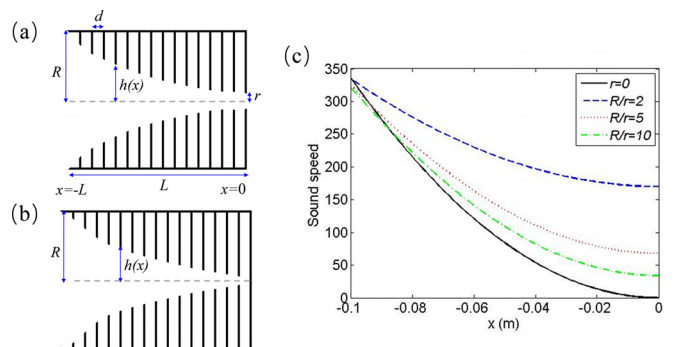

FIG. 2. (a) Sound transmission through the ABH in a one-dimensional duct. (b) ABH with closed-end termination, $r = 0$; (c) Decay behavior of sound speed along the length of the ABH, with respect to different r to R ratios.

The phase and group velocities of sound wave propagation are, respectively,

$$c_{ph} = \frac{\omega}{k} = \frac{\omega[(R-r)x^2 + rL^2]}{\sqrt{k_0^2 R^2 L^4 - 4(R-r)^2 x^2}};$$

$$c_g = \left(\frac{\partial k}{\partial \omega}\right)^{-1} = \frac{c_0^2[(R-r)x^2 + rL^2]\sqrt{k_0^2 R^2 L^4 - 4(R-r)^2 x^2}}{\omega L^4 R^2}. \tag{6}$$

In the special case where the end termination is fully closed with $r = 0$, the wavenumber expression Eq. (5) becomes

$$k(x) = \frac{1}{x^2}\sqrt{k_0^2 L^4 - 4x^2}. \tag{7}$$

This also applies to the condition where the radius of the opening is much smaller than the initial duct radius, i.e., $r \ll R$. It can be seen that as the wave approaches the end, the local wavenumber k at $x = 0$ will increase to infinity. At the entrance, $x = -L$, the wavenumber is $k(-L) = \frac{1}{L^2}\sqrt{k_0^2 L^4 - 4L^2}$. With the incoming wave frequency f increased to $k_0^2 L^4 \gg 4L^2$, i.e., $f \gg c_0/\pi L$, the wavenumber can be approximated as $k = k_0$. In such a case, the smooth variation of the local wavenumber from k_0 to infinity ensures matched impedance from the entrance to the end for sound waves to fully enter the ABH. Mathematically, this condition is fulfilled by imposing the cross-sectional variation and wall impedance variation together, as described in Eq. (4).

As a numerical example, we investigate an ABH with $R = 30$ mm and $L = 100$ mm. The radius R is equal to that of an impedance tube, which will be used later for the measurement, and length L allows a clear wave trapping effect in the measurable frequency range between 1000 and 6000 Hz. The inner duct and cavities in-between the rings are filled with air with $\rho_0 = 1.213$ kg/m^3 and $c_0 = 340$ m/s. The local sound speed (both phase and group velocities) as calculated from Eq. (7) shows a smooth decaying pattern along the ABH positions from $x = -L$ to $x = 0$. This means that wave propagation is progressively slowed down while traveling toward the end. With a closed end $r = 0$, the structure can fully reduce the sound speed to zero, making it an ideal situation for complete wave trapping as the wave-front will never reach the end. As for the sound transmission configurations with different r to R ratios, it can be seen that the slope of the sound speed decay is faster with a greater R/r. If the radius of the opening is half of the duct radius, $R/r = 2$, the sound speed is only mildly slowed down. Strong reflection or transmission can be expected, depending on whether the end termination is closed or opened. With a bigger R to r ratio, e.g., $R/r = 10$, the sound speed is decreased by ten times, evidencing the occurrence of the strong ABH effect to impair sound reflection and transmission simultaneously.

As the quadratic profile does not allow explicit analytical solution, we adopt the TMM to compute the sound transmission and reflection coefficients. The TMM formulation is summarized in the supplementary material. Referencing to Fig. 3, the ABH structure is discretized into $N = 40$ pairs of air columns called cylinders, such that the length of each discretized duct segment is $d = 2.5$ mm. The number of rings is sufficient to provide a smooth variation and approximation of the tapered profile and the required impedance change, as stipulated in the analytical derivation.[16-18] The radius of the duct is
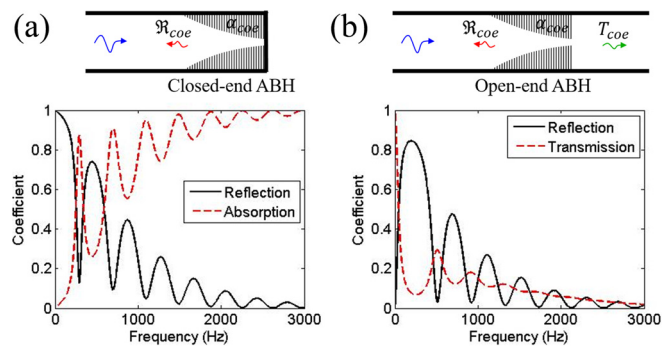
FIG. 3. (a) Reflection and absorption coefficients of the closed-end ABH with rigid termination. (b) Reflection and transmission coefficients of the ABH with open termination. Strong decay of the reflection coefficient can be observed in both figures due to the ABH effect.

the same as the one used in the above theoretical analysis, i.e., $R = 30$ mm. The duct cutoff frequency is calculated as $f_c = 1.84c_0/(2\pi R) = 3000$ Hz, below which the plane wave assumption remains valid. The termination radius is taken as 1/10 of the initial duct radius, $r = R/10 = 3$ mm. The damping effect is taken into consideration by using a complex sound speed, $c = c_0(1 + 0.05j)$, where 0.05 is the assumed damping loss factor. This roughly estimates the viscothermal loss between the narrow rings and allows the trapped energy to be dissipated. Note that more accurate damping conditions such as containing foams can be analyzed by introducing the porous material model.[17]

The reflection and absorption coefficients with a closed-end configuration are first plotted in Fig. 3(a). The velocity at the end termination is zero due to the hard boundary, and the reflection coefficient can be calculated from Eq. (S4) in the supplementary material. The frequency range is chosen from 10 to 3000 Hz, below the duct cutoff frequency. It can be seen that sound reflection is strong at the low frequency, which gradually decreases to nearly zero at higher frequencies, despite some oscillating behavior. The fluctuation is related to the geometric settings including the number of discretized cylinders, total length, and the assigned damping loss factor, as analyzed by the previous paper.[17] The frequency where the reflection coefficient starts to decrease rapidly can be linked to the ABH length L, roughly from $c_0/\pi L = 1082$ Hz. The length of the ABH (100 mm) is 1/3 of the acoustic wavelength at this frequency (314 mm). The most interesting feature of the ABH effect is that after this frequency threshold, the reflection coefficient maintains a very low profile toward high frequencies. Such behavior is drastically different from traditional resonant absorbers, whose effective frequency is closely related to the resonance embedded in the absorber and only spans over a very narrow frequency band.[12-15] This clearly shows the advantage of the ABH as a result of the wave trapping effect. As the absorption coefficient is defined as $\alpha_{coe} = 1 - |\Re|^2$, it follows that the α_{coe} curve remains greater than 0.9 above 1500 Hz, which is also a remarkable performance as the total ABH length is only 100 mm.

An open-end ABH is then investigated. The geometric parameters are exactly the same as those used in the above closed-end case, except that the termination connects to an open duct of radius R. In comparison to the closed-end, the open-end ABH shows a similar

decay behavior in terms of the sound reflection coefficient as shown in Fig. 3(b). The difference exists in the low frequency range where the reflection coefficient of the closed-end ABH starts from one, while the open-end ABH starts from zero. The reversed behavior is because the open-end ABH permits sound transmission rather than reflection before the ABH effect takes place. Again, above $c_0/\pi L = 1082$ Hz, we observe a rapid decrease in the reflection coefficient, as the ABH generates both impedance matching and slow-sound effects for perfect sound trapping. The transmission coefficient T_{coe} describing the amount of sound energy that can leave from the ABH also shows a substantial decay. As energy is conservative, the drop of both reflection and transmission simply means that sound energy is trapped in the ABH structure and is eventually dissipated by the damping in the system. The ABH, therefore, acts as an energy sink. Here, it is worth mentioning that the open-end ABH demonstrates superior reflection-proof and transmission-proof behavior. This is conducive to noise control or acoustic wave manipulation, as little sound waves will be bounced back to the source side, which could jeopardize the overall performance.
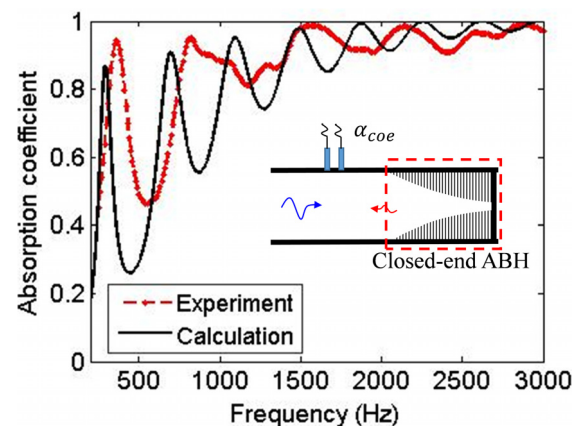
Finally, we present experimental results on an ABH prototype based on the impedance tube measurement. The prototype adopts the same geometric parameter as that used in the preceding analyses. The prototype was 3D printed (Original Prusa i3 MK3S+, SLA resin). The total ABH length $L = 100$ mm is divided into $N = 40$ rings, and its inner structure follows the quadratic profile design as shown in Fig. 1(b). As the printed wall thickness is 1 mm, the actual air cavity width between each pair of rings is 1.5 mm. Note that the narrow cavities present inherent viscous damping, so that no additional damping material is actually needed herein. Figure 4(a) shows the printed sample and the test-rig used to measure the sound reflection and transmission. An impedance tube (SW477 impedance tube, BSWA) with an inner radius of $R = 30$ mm is used, where two pairs of microphones are flush-mounted at upstream and downstream, respectively, to measure the reflected sound wave and transmitted sound wave strengths. The measurable range of the impedance tube system is between 200 and 3000 Hz.
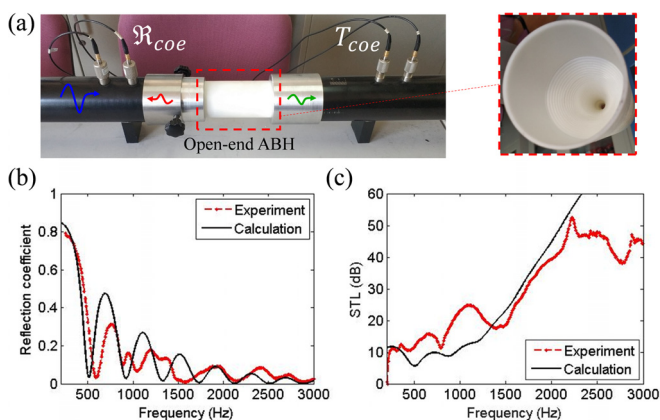
The measured reflection coefficient and the calculated one using the TMM are compared in Fig. 4(b), where good agreement in terms of general trend and magnitude can be observed. The observed discrepancies can mainly be attributed to the neglected wall thickness in the TMM calculation and the air damping estimation. The experimentally measured Sound Transmission Loss (STL), defined as the inverse of the transmission coefficient on a logarithmic scale, $STL = 10\log(1/T_{coe})$, is plotted in Fig. 4(c). Note that STL on the dB scale is more suitable to describe the noise attenuation capacity than the transmission coefficient, as the latter is defined in percentage of energy. It can be seen that the STL of the open-end ABH shows a remarkable sound attenuation greater than 10 dB over nearly the entire frequency range considered here. Above 1082 Hz, the STL curve shows a continuous increasing trend, peaked at around 2200 Hz followed by a plateau region with a very high STL level of roughly 40 dB. Ideally, as the ABH effect has fully developed in this frequency range, the sound propagation should, in principle, be completely suppressed, ideally making the STL to continue to rise. However, a further STL increase may be limited by other factors such as structural-acoustical coupling through wall vibration, which are inevitable in experiment. Finally, the printed sample is placed in a standard two-microphone impedance tube with a rigid backing, where the absorption coefficient of the closed-end ABH is measured. Figure 5 shows the experiment result and its comparison with the TMM calculation. The agreement is reasonable in terms of general variation tendency, and the discrepancies can be attributed to the same reasons as explained above in terms of damping estimation and the ignorance of the partition wall thickness. Nevertheless, the ABH-specific sound absorption is confirmed. It is worth noting that the proposed ABH design can achieve a high STL and high absorption without relying on any sound absorbing material. Adding porous material to the ABH may provide an extra benefit, which can be further explored in future studies.

In conclusion, the sound transmission and reflection characteristics of air-filled ABH are investigated. The most prominent feature of the sonic ABH design is that the local sound speed is progressively slowed down as the wave propagates, before eventually being trapped inside the ABH without being reflected back or transmitted downward. The condition governing the occurrence of the sonic ABH

FIG. 4. (a) Experimental rigs to measure the sound reflection and transmission coefficient of an open-end ABH using an impedance tube. (b) Comparison between the measured reflection coefficient and the TMM calculation. (c) Experimentally measured Sound Transmission Loss of the open-end ABH prototype.

FIG. 5. The measured sound absorption coefficient of a closed-end ABH with rigid backing and its comparison with the TMM calculation.

phenomena is fulfilled by combining a smooth decrease in the cross-sectional area with a matched variation of the wall admittance of the sonic ABH device. Experiments confirm the existence of the ABH effect in drastically reducing the sound reflection. At the same time, sound transmission is proportionally decreased with the ABH acting as an energy sink, focalizing and extracting energy out of the system.

It is worth mentioning that the ABH structure does not require damping material in its original format. The slow-sound and wave trapping effects do not rely on particular damping treatment although a small damping loss factor is introduced in the TMM calculation. Should additional damping be necessary, a small amount of damping materials near the tip region would be effective as the energy is mostly trapped there. The presented experiment shows that without using any additional porous material, the inherent air damping in the narrow cavities alone is already sufficient.

The effective frequency range of the ABH only has a lower bound. After a certain frequency, which is determined at $c_0/\pi L$ based on the current analyses, a typical ABH effect exhibits, the consequence of which is showcased by reduced sound reflection and transmission down to a very minimal level, persistent at high frequencies. These appealing features are absent in existing resonant-type sound absorbers. The theory proposed and the properties of the ABH presented in this paper can inspire the development of new noise control devices, applicable to many practical systems such as nozzle, muffler, and even metasurface with ABH cells with proper arrangement.

See the supplementary material for details about the transfer matrix method (TMM) used for the calculation of reflection and transmission coefficients of the proposed ABH structure.

DATA AVAILABILITY

The data that support the findings of this study are available from the corresponding author upon reasonable request.

REFERENCES

[1] A. Pelat, F. Gautier, S. C. Conlon, and F. Semperlotti, J Sound Vib **476**, 115316 (2020).

[2] M. A. Mironov, Sov. Phys. Acoust. **34**(3), 318–319 (1988).

[3] V. V. Krylov and F. J. B. S. Tilman, J. Sound Vib. **274**(3), 605–619 (2004).

[4] V. Denis, F. Gautier, A. Pelat, and J. Poittevin, J. Sound Vib. **349**, 67–79 (2015).

[5] H. Ji, J. Luo, J. Qiu, and L. Cheng, Mech. Syst. Signal Process. **104**, 19–35 (2018).

[6] L. Tang and L. Cheng, Appl. Phys. Lett. **109**(1), 014102 (2016).

[7] J. Leng, V. Romero-García, A. Pelat, R. Picó, J. P. Groby, and F. Gautier, J. Sound Vib. **471**, 115199 (2020).

[8] S. C. Conlon, J. B. Fahnline, and F. Semperlotti, J. Acoust. Soc. Am. **137**(1), 447–457 (2015).

[9] P. A. Feurtado and S. C. Conlon, J. Acoust. Soc. Am. **142**(3), 1390–1398 (2017).

[10] J. Y. Lee and W. Jeon, J. Acoust. Soc. Am. **141**(3), 1437–1445 (2017).

[11] J. Deng, L. Zheng, P. Zeng, Y. Zuo, and O. Guasch, Mech. Syst. Signal Process. **118**, 461–476 (2019).

[12] D.-Y. Kim, J.-G. Ih, and M. Åbom, J. Sound Vib. **466**, 115045 (2020).

[13] X. Wang and C.-M. Mak, J. Acoust. Soc. Am. **131**(2), 1172–1182 (2012).

[14] X. Yu, L. Cheng, and X. You, J. Acoust. Soc. Am. **137**(2), 951–962 (2015).

[15] X. Zhang and L. Cheng, Appl. Acoust. **167**, 107382 (2020).

[16] M. Mironov and V. Pislyakov, Acoust. Phys. **48**, 347 (2002).

[17] O. Guasch, M. Arnela, and P. Sánchez-Martín, J. Sound Vib. **395**, 65–79 (2017).

[18] J. P. Hollkamp and F. Semperlotti, J. Sound Vib. **465**, 115035 (2020).

[19] J. Zhu, Y. Chen, X. Zhu, F. J. Garcia-Vidal, X. Yin, W. Zhang, and X. Zhang, Sci. Rep. **3**, 1728 (2013).

[20] N. Jiménez, V. Romero-García, V. Pagneux, and J.-P. Groby, Sci. Rep. **7**, 13595 (2017).

[21] T. Liu, S. Liang, F. Chen, and J. Zhu, J. Appl. Phys. **123**(9), 091702 (2018).

[22] A. A. El Ouahabi, V. V. Krylov, and D. J. O'Boy, in Proceedings of the 22nd International Congress on Sound and Vibration (2015).